Journal of Pharmaceutical Analysis 10 (2020) 482–489

Contents lists available at ScienceDirect

Journal of Pharmaceutical Analysis

journal homepage: www.elsevier.com/locate/jpa

Original article

A carbon nanoparticle-peptide fluorescent sensor custom-made for simple and sensitive detection of trypsin

Shanshan Hou [a, 1], Tingting Feng [c, 1], Na Zhao [a], Jiaxin Zhang [a], Huibin Wang [a], Ning Liang [b, **], Longshan Zhao [a, *]

[a] School of Pharmacy, Shenyang Pharmaceutical University, Shenyang, Liaoning Province, 110016, China
[b] School of Pharmaceutical Engineering, Shenyang Pharmaceutical University, Shenyang, Liaoning Province, 110016, China
[c] Institute of Pharmaceutical and Food Engineering, Shanxi University of Chinese Medicine, Jinzhong, Shanxi Province, 030619, China

ARTICLE INFO

Article history:
Received 9 February 2020
Received in revised form
20 August 2020
Accepted 20 August 2020
Available online 27 August 2020

Keywords:
Carbon nanoparticles
Fluorescence quenching
Förster resonance energy transfer (FRET)
Fluorescein-labelled peptide
Trypsin assay

ABSTRACT

Herein, we report a novel sensor to detect trypsin using a purpose-designed fluorescein-labelled peptide with negatively charged carbon nanoparticles (CNPs) modified by acid oxidation. The fluorescence of the fluorescein-labelled peptide was quenched by CNPs. The sensor reacted with trypsin to cleave the peptide, resulting in the release of the dye moiety and a substantial increase in fluorescence intensity, which was dose- and time-dependent, and trypsin could be quantified accordingly. Correspondingly, the biosensor has led to the development of a convenient and efficient fluorescent method to measure trypsin activity, with a detection limit of 0.7 μg/mL. The method allows rapid determination of trypsin activity in the normal and acute pancreatitis range, suitable for point-of-care testing. Furthermore, the applicability of the method has been demonstrated by detecting trypsin in spiked urine samples.

1. Introduction

Trypsin, an extremely important pancreatic digestive enzyme, is produced in the pancreas and plays crucial roles in the small intestine. Under abnormal circumstances, trypsin can hydrolyze various pancreatic zymogens, such as carboxypeptidase, phospholipase, and chymotrypsinogen into their active forms, and control the secretory function of the pancreas [1]. Pancreatic secretory trypsin inhibitor (PSTI) produced by the pancreas can effectively inhibit trypsin activity [2]. However, once trypsin activation exceeds PSTI control, various other proteases are activated to begin self-digestion, which damages cells and leads to many diseases such as pancreatitis [3], intestinal obstruction [4], and even pancreatic cancer [5]. Thus, the establishment of a facile and rapid method for the identification and detection of trypsin is crucial for effective diagnosis and treatment of pancreatic diseases. Recently, many efforts have been reported regarding trypsin determination; for example, Seia et al. [6] developed a silica nanoparticle-based fluorescence platform to detect immunoreactive trypsin (IRT) in cystic fibrosis (CF) newborn screening. Additionally, Lou et al. [7] reported a colorimetric assay for trypsin based on a copper ion chemical detector. Dong et al. [8] proposed an electrochemical method by employing a heptapeptide as a substrate to detect trypsin. In the work of Shi et al. [9], a "turn-on" system based on CdTe Quantum Dots, for trypsin assay was proposed. Unfortunately, these experimental methods invariably require complicated experimental manipulation, long time, expensive and toxic materials, and large-volume samples. Therefore, it remains a challenge to establish facile, cost-effective, and sensitive methods for the detection of trypsin.

It is well known that certain carbon nanomaterials, including graphene, fullerene, carbon nanotubes, and carbon nanofibers, among others, have attracted much attention at the frontiers of technological innovation as drug delivery carriers due to their excellent electrochemical, optical, mechanical biocompatibility, thermal and adsorption properties [10–12]. Nevertheless, there are relatively few studies regarding carbon nanoparticle materials compared to the above carbon-based materials. Since Liu et al. [13] proposed the use of candle soot to prepare fluorescent carbon nanoparticles (CNPs), the characteristics of such soot have been

Peer review under responsibility of Xi'an Jiaotong University.
* Corresponding author.
** Corresponding author.
E-mail addresses: liangning@syphu.edu.cn (N. Liang), longshanzhao@163.com (L. Zhao).
[1] Shanshan Hou and Tingting Feng contributed equally.

https://doi.org/10.1016/j.jpha.2020.08.009

studied gradually. Many different methods have been applied to synthesizing CNPs as reported over recent years, such as hydrothermal [14], chemical oxidation [15], laser ablation [16], microwave heating [17], auxiliary synthesis [18], and electrochemical oxidation [19]. Nonetheless, the luminescent CNPs prepared by these methods have low quantum yield and wide half-width, which greatly limit their widespread application. According to the properties of carbon materials and nano-scale size effects, CNPs exhibit strong interactions with dye molecules which have planar structures, and fluorescence quenching can result from electron or energy transfer [20]. Thus, we have conducted research concerning CNPs with large particle sizes, and which are non-fluorescent, chemically inert, nontoxic, and biocompatible [21]. CNPs were prepared by a nitric acid oxidation method. In order to render candle soot, which has poor dispersibility in aqueous solutions, fuller contact with nitric acid, we dispersed the candle soot in N, *N*-dimethylformamide (DMF) to completely oxidize the surfaces of the CNPs in the first time. Accordingly, using CNPs as fluorescence quenching agents, we suggested a fluorescence method for the determination of trypsin based on the principle of Förster resonance energy transfer (FRET).

The design strategy for the CNP-peptide fluorescence sensor is outlined in the accompanying graphical abstract. A peptide containing six arginine residues was chosen as a sensitive trypsin substrate, because recent studies have identified that this peptide can be selectively cleaved by trypsin [22,23]. The surface of CNPs oxidized by nitric acid has more negatively charged groups such as COO^- and OH^- [24]. Specifically, a 5-carboxy-fluorescein (FAM)-labelled peptide containing Arg_6 was synthesized. After that, mixtures of the dye-labelled peptide and CNPs self-assembled to form the two components through electrostatic interactions. As a consequence, effective FRET occurred between FAM and CNPs, with solution fluorescence being quenched. After reacting with trypsin, the self-assembled peptides were cleaved by the protease, and Arg_6-FAM was released from CNP surfaces, resulting in fluorescence recovery. The determination of trypsin content is quantitatively based on the enhanced fluorescence intensity. Hence, after a further introduction of the inhibitor, dissociation of the sensor will be prevented, and the fluorescence will change accordingly [25,26]. Subsequently, it has been demonstrated that the sensor has high sensitivity and accuracy in detecting trypsin content. In addition, the modified probe was successfully applied to the quantitative analysis of trypsin in urine samples. As a consequence, this study not only broadens the application of fluorescence analysis of CNPs, but also provides a new scientific method for patients to achieve rapid and effective screening of early pancreatitis.

2. Experimental

2.1. Reagents and chemicals

Ordinary candles were purchased from a school supermarket, 98% nitric acid and N, *N*-dimethylformamide (DMF) were purchased from Tianjin Fuyu Fine Chemical Co., Ltd. (Tianjin, China), and Arg_6-FAM peptide was purchased from Shanghai Renjie Biotechnology Co., Ltd (Shanghai, China). Trypsin (1:2500) from porcine pancreas was purchased from Beijing Bailingwei Technology Co., Ltd. (Beijing, China), and Bowman-Birk protease inhibitor was purchased from TCI Development Co., Ltd. (Shanghai, China). Lysozyme, thrombin, pepsin, and IgG antibodies were obtained from Beijing Solarbio Science & Technology Co., Ltd. (Beijing, China). All chemicals obtained from commercial sources were of analytical grade and could be used without further purification. Stock solutions were prepared using phosphate buffered saline (PBS) (2.0 mM, pH = 8, Ca^{2+} = 10 μM). The PBS was prepared by mixing an aqueous Na_2HPO_4 solution with sodium hydroxide.

2.2. Instrumentation

Fluorescence spectra were recorded on a fluorescence spectrophotometer (Tianjin, China) at an excitation wavelength of 490 nm and an emission wavelength between 500 and 700 nm. The excitation and emission slits were 5 nm wide, and photomultiplier tube (PMT) voltage was 500 V. Transmission electron microscopy (TEM) images were captured on a JEM2100F electron microscope operated at 200 kV (JEOL, Japan). Scanning electron microscopy (SEM) measurements were performed on a Zeiss Supra 55 scanning electron microscope. ζ-potentials were measured using a Malvern Nano ZS instrument (Malvern, UK). CNP functional groups were further confirmed via a Nicolet 6700 Fourier transform infrared (FT-IR) spectrometer (Bruker, Germany).

2.3. Synthesis of CNPs

Dry candle soot weighing 4.5 mg was placed in a 10 mL round bottom flask and dissolved in 2 mL DMF and 2 mL 98% nitric acid. A condenser pipe was connected to the flask, with a balloon over the upper end of the condenser pipe. After that, the mixture was stirred in an oil bath at 140 °C for a period of 12 h. The reaction solution was poured into a 5 mL centrifuge tube and centrifuged so as to separate into two layers. The upper layer of liquid was yellow, while the lower layer was black. After removing the upper layer, distilled water was added and mixed evenly, and then centrifuged at 4000 rpm for 4 min. This step was repeated five times until the carbon nanoparticle solution pH = 7. The CNPs were dispersed in distilled water at a concentration of 0.5 mg/mL for further characterization and use.

2.4. Characterization

As shown in Fig. 1A, it can be seen that the candle soot obtained by combustion was completely insoluble in water, whereas the CNPs obtained by the nitric acid oxidation treatment could be uniformly dispersed in the aqueous solution. On the one hand, it may be because the candle soot is hydrophobic and on the other hand, the candle soot is crosslinked together into larger particles that are insoluble in water [27,28]. After oxidation by nitric acid, the surface groups of the CNPs were changed, and hydrophilic groups such as −COOH and −OH were generated, so the dispersion effect in the aqueous solution was good.

Morphological characterization of synthesized CNPs was determined using SEM and TEM. From SEM and TEM images (Figs. 1B and C), it can be seen that the synthesized CNPs were evenly distributed. We measured the size of 280 CNPs in 4 projected electron microscopy images [29,30]. The approximate size distribution of CNPs ranged from 20 to 70 nm, most of which were 30 nm, as illustrated in Fig. 1C. It demonstrated that the CNPs oxidized by nitric acid were still present as larger particles. Since the CNPs diameters were >10 nm and could not emit fluorescence, it was considered to be suitable as a quenching agent.

According to the Zeta potential distribution diagram in Fig. 1D, it can be found that the Zeta potential of CNPs was negative, indicating that COO^- and OH^- moieties may be generated on the oxidized CNP surfaces, resulting in an increase in negatively charged groups. At the same time, the Zeta potential can greatly affect the stability of ions through electrostatic repulsion between particles [31,32]. The Zeta potential of CNPs was (−35.4 ± 5.42) mV. The Zeta potential in this range overcomes the tendency of natural aggregation and has high stability.

FT-IR spectra revealed bonding configurations and functional group information regarding CNPs (Fig. 1E). The peaks at

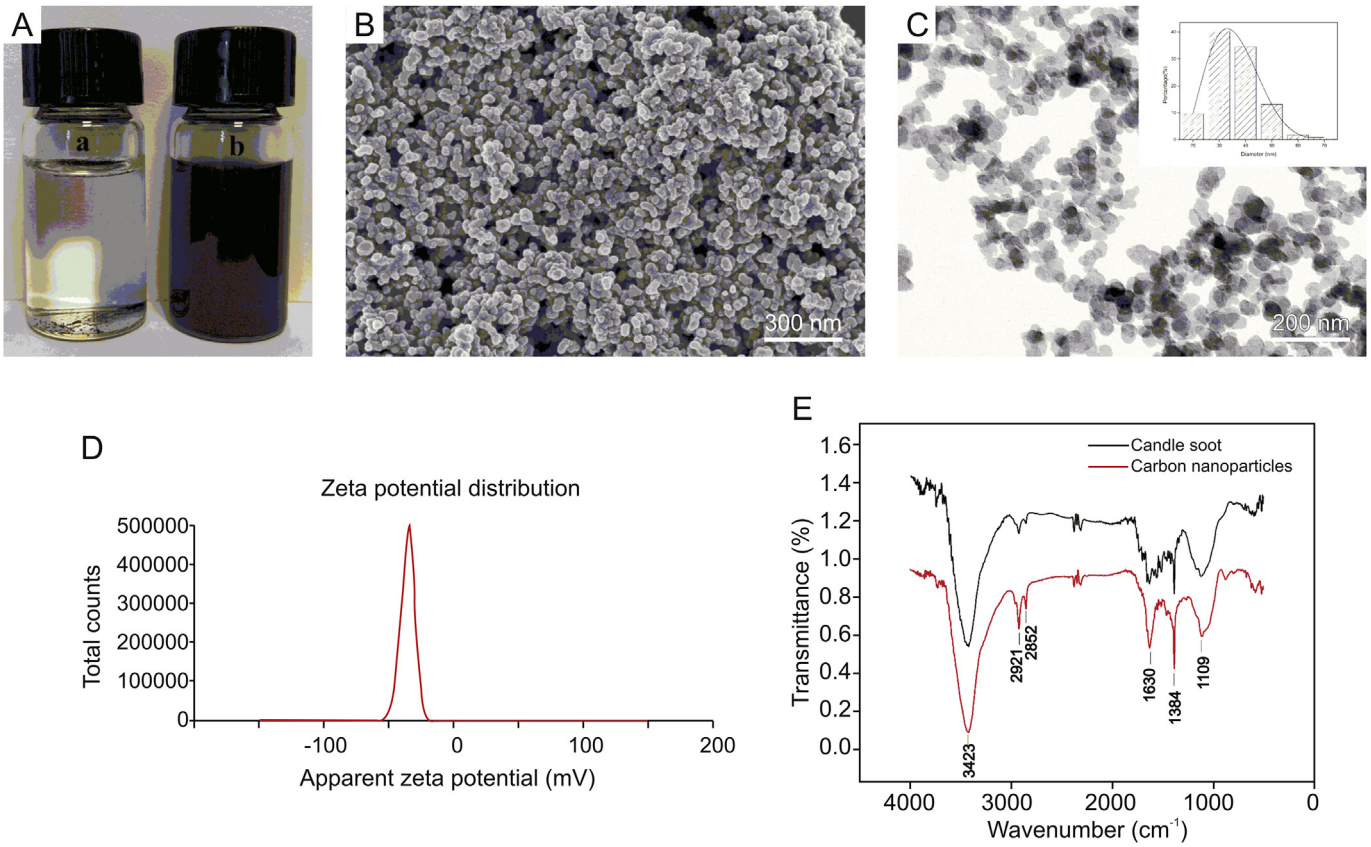

Fig. 1. (A) Dispersion of unoxidized candle soot and oxidized carbon nanoparticles (CNPs) in aqueous solution (a, b); (B) SEM image of CNPs; (C) TEM images of CNPs: the inset indicates the particle size distribution of carbon nanoparticles; (D) Zeta potential diagram of CNPs; and (E) FT-IR spectra of CNPs.

approximately 3423 and 1109 cm^{-1} can be ascribed to the characteristic absorption bands of the −OH stretching vibration mode. Compared with the FT-IR spectrum of candle soot before oxidation, the peak at 1630 cm^{-1} could be attributed to the asymmetric stretching vibration of −C=O. The characteristic $-CH_2-$ absorption band of stretching at 2921-2958 cm^{-1} could also be observed, and the peak at 1384 cm^{-1} can be assigned to the C−H stretching mode [33,34]. The above observations confirmed that the synthesized nanoparticles were surface functionalized with hydroxyl and carboxylic/carbonyl moieties, which is consistent with the reason for the change of Zeta potential previously studied.

2.5. Fluorescence quenching of peptides

CNPs stock solution (0.5 mg/mL) was added to dissolved Arg_6-FAM [0.1 nM PBS (2.0 mM, pH = 8.0, $[Ca^{2+}] = 10$ μM)] to obtain the desired CNP concentration [35]. Using solutions of 0−32 μg/mL, fluorescence spectra of each solution were recorded. In addition, CNPs stock solution (0.5 mg/mL) was added to dissolved Arg_6-FAM [0.1 nM PBS (2.0 mM, pH = 8.0, $[Ca^{2+}] = 10$ μM)]. A solution with a maximum quenching concentration of CNPs of 20 μg/mL was obtained, and then the fluorescence intensity of the solution at 520 nm was recorded between 0 and 35 min.

2.6. CNPs/Arg_6-FAM trypsin assays

Trypsin stock solution (0.2 mg/mL) was added to 2.0 mL of CNPs/Arg_6-FAM{[Arg_6-FAM] = 0.1 nM and [CNPs] = 20 μg/mL in PBS (2.0 mM, pH = 8.0, $[Ca^{2+}] = 10$ μM)}. A series of solutions with trypsin concentrations of 1, 1.5, 2, 10, and 20 μg/mL was obtained. Each solution was incubated at 37 °C for 0−35 min, and fluorescence intensity at 520 nm was recorded. Trypsin stock solution (0.2 mg/mL) was added to 2.0 mL of CNPs/Arg_6-FAM{[Arg_6-FAM] = 0.1 nM and [CNPs] = 20 μg/mL in PBS (2.0 mM, pH = 8.0, $[Ca^{2+}] = 10$ μM)}. A series of solutions with trypsin concentrations ranging from 0 to 30 μg/mL was obtained. Each solution was incubated at 37 °C for 30 min and fluorescence spectra were recorded.

2.7. Trypsin inhibition by BBI using the CNPs/Arg_6-FAM ensemble

BBI was added to 2.0 mL of CNPs/Arg_6-FAM solution {[Arg_6-FAM] = 0.1 nM and [CNPs] = 20 μg/mL in PBS (2.0 mM, pH = 8.0, $[Ca^{2+}] = 10$ μM)}, a series of solutions with BBI concentrations of 0, 0.2, 0.5, 1, 2, 3, 4, 5, and 6 μg/mL was obtained. To each of the above solutions, 100 μL of trypsin (0.2 μg/mL) was added. Each solution was incubated at 37 °C for 30 min, and the fluorescence intensity at 520 nm was recorded.

2.8. Selectivity

Under the above-mentioned optimum experimental conditions, four different proteins, namely, thrombin, pepsin, lysozyme, and IgG, each at a final concentration of 10 μg/mL, were prepared and incubated with CNPs/Arg_6-FAM to study selectivity of the assay. 10 μg/mL of trypsin was used as a positive control, and all emission ratios were normalized. The emission spectra of the resultant mixtures were directly measured with excitation at 490 nm, and the fluorescence recovery efficiency was also calculated.

2.9. Urine sample preparation and trypsin determination

The performance of this fluorescence method for the determination of trypsin was investigated under optimal conditions. Urine samples were diluted 10-fold, and used directly for measurement without other pretreatment processes. Different concentrations of trypsin were added to the diluted urine samples from healthy subjects, and fluorescence spectra were recorded at 30 min.

3. Results and discussion

3.1. Interaction between CNPs and Arg_6-FAM

First, the amount of CNPs used as Arg_6-FAM quencher was optimized. As can be seen in Fig. 2A, peptide solutions with FAM exhibited strong fluorescence in the absence of CNPs. The fluorescence intensity of the solution gradually weakened as the concentration of CNPs increased. Up to 99% of the fluorescence could be quenched when the concentration of CNPs was increased to 20 μg/mL. Consequently, it indicated that CNPs underwent strong interactions with the peptide, and could efficiently quench the fluorescence. This quenching may be ascribed to the efficient energy transfer from FAM to the CNPs [36].

Meanwhile, as shown in Fig. 2B, by monitoring changes in fluorescence intensity over time, the kinetic behavior of the CNP-peptide complex formation was also studied (Fig. 2B). The above-mentioned maximum quenching concentration of CNPs was added to the Arg_6-FAM solution, and the fluorescence intensity of the CNPs-peptide complex solution at 520 nm was recorded from 0 to 35 min [37]. After adding CNPs, the fluorescence of the peptide dropped rapidly and reached a constant level within 1 min, indicating that the binding of the peptide to CNPs is a rapid and stable process.

We performed fluorescence quenching experiments with Arg_6-FAM using CNPs, and Fig. 2C shows a gradual decrease in fluorescence intensity of Arg_6-FAM after addition of CNPs to the solution. The Arg_6-FAM solution showed a presented fluorescence emission spectrum in the absence of CNPs (Fig. 2C, curve a). Nevertheless, after addition of CNPs (20 μg/mL), fluorescence quenching of up to 99.2% was observed (Fig. 2C, curve b). This change in fluorescence was recognizable by the naked eye. In the absence and presence of CNPs, a photo of Arg_6-FAM in a PBS solution under UV light irradiation was shown in the inset of Fig. 2C. The fluorescence quenching process does not involve emission and reabsorption of photons; hence it is non-radiative, and effective energy transfer is achieved by FRET through dipole-dipole coupling [38,39]. Electrostatic interactions between arginine containing FAM and negatively charged

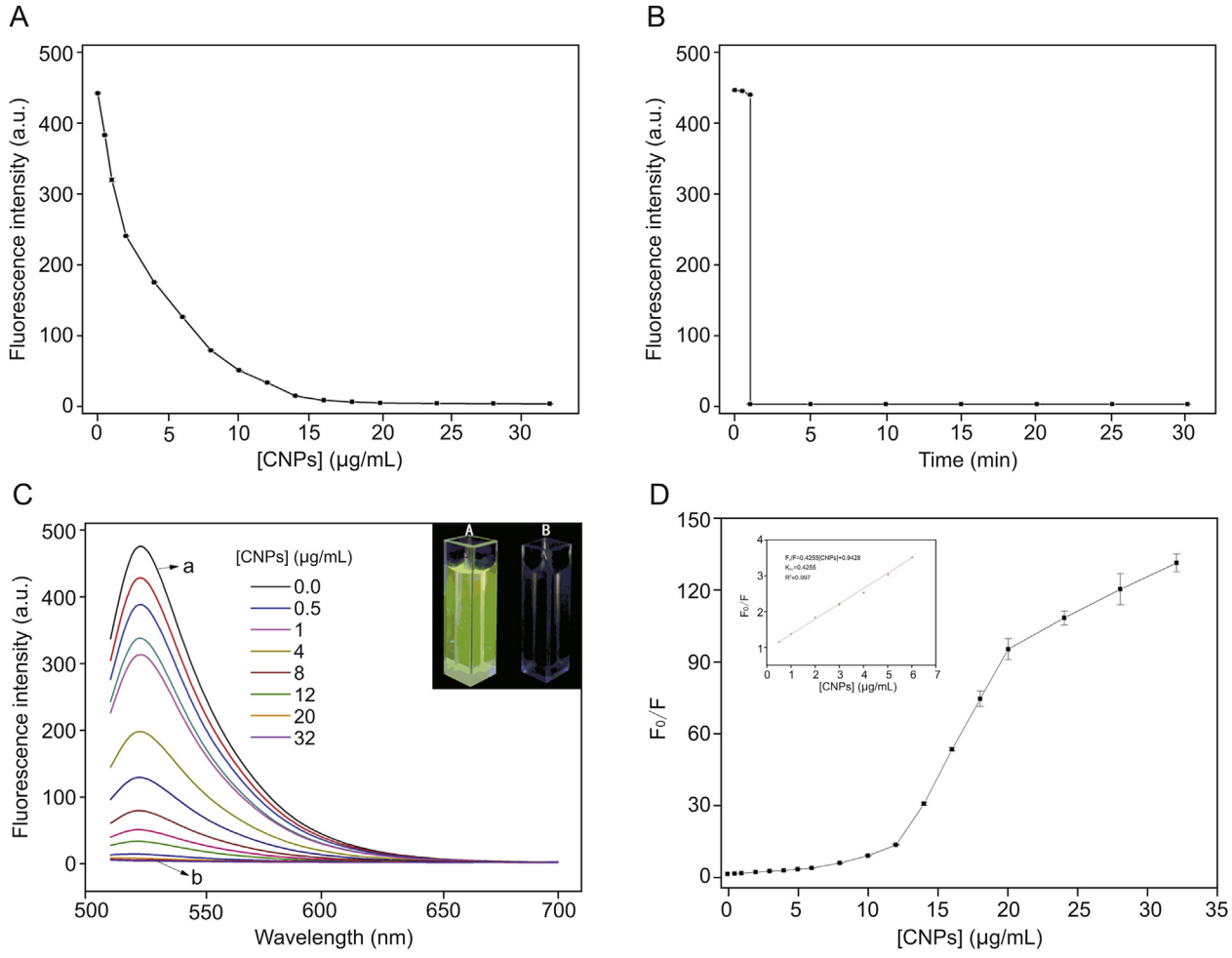

Fig. 2. (A) Fluorescence quenching intensity of Arg_6-FAM (0.1 nM) in the presence of different concentrations of CNPs; (B) Fluorescence quenching of Arg_6-FAM (0.1 nM) by CNPs (20 μg/mL) in PBS (2.0 mM, pH = 8.0, $[Ca^{2+}]$ = 10 μM) as a function of time; (C) Fluorescence spectra of Arg_6-FAM (0.1 nM) after addition of different amounts of CNPs. The inset shows photographs of (A) Arg_6-FAM and (B) Arg_6-FAM and CNP solutions under UV (365 nm) illumination; and (D) Variation of fluorescence intensity ratios (F_0/F) at 520 nm versus the concentration of CNPs. The inset shows the near-linear plot of the fluorescence intensity ratios (F_0/F) at 520 nm versus the concentration of CNPs (0.5, 1.0, 2.0, 3.0, 4.0, 5.0, and 6.0 μg/mL) for solutions in which the concentrations of CNPs were minimal. All samples were prepared with PBS (2.0 mM, pH = 8.0, $[Ca^{2+}]$ = 10 μM), and the excitation wavelength employed was 490 nm.

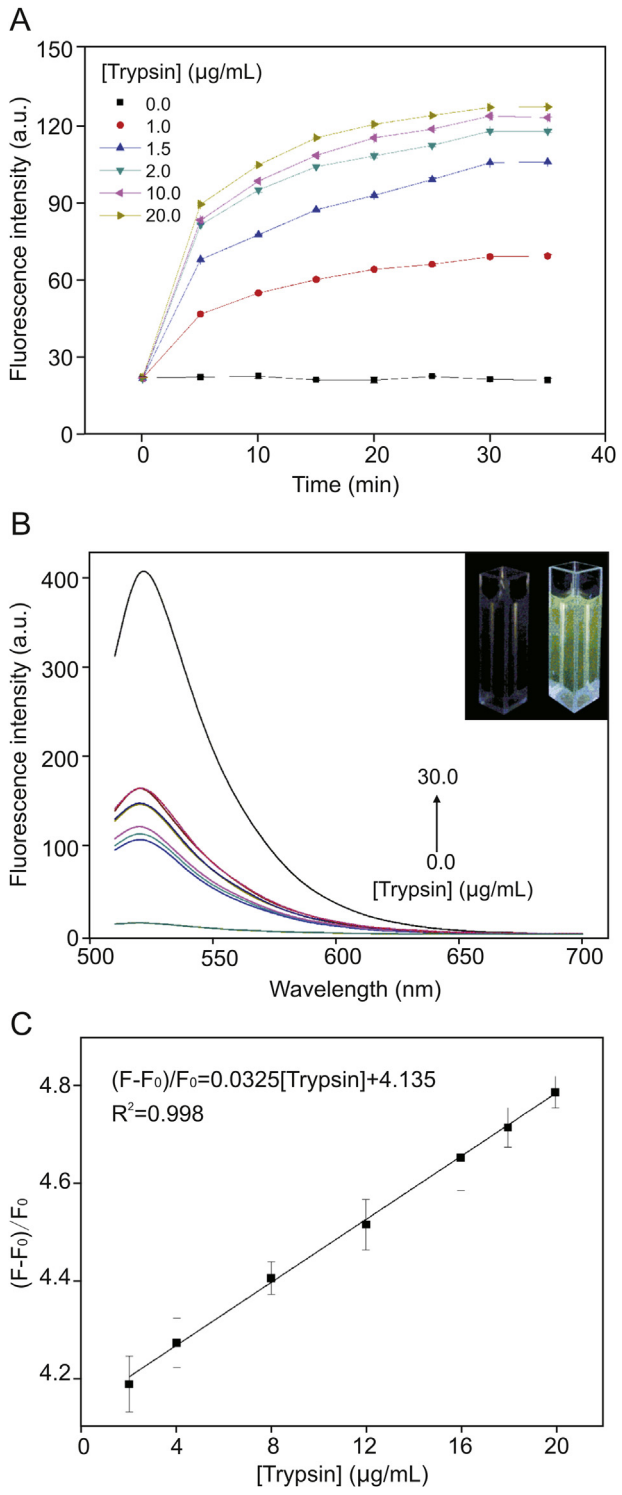

Fig. 3. (A) Plots of fluorescence intensity at 520 nm versus reaction time for the Arg_6-FAM (0.1 nM) and CNP (20 μg/mL) ensemble in the presence of different concentrations of trypsin (1.0, 1.5, 2.0, 10.0, and 20.0 μg/mL). All samples were prepared in PBS (2.0 mM, pH = 8.0, $[Ca^{2+}]$ = 10 μM), and the excitation wavelength employed was 490 nm; (B) Fluorescence spectra of different concentrations of trypsin and Arg_6-FAM (0.1 nM) and CNPs (20 μg/mL) after incubation at 37 °C for 30 min; (C) Linear relationship between fluorescence recovery and concentration of trypsin within the range of 2–20 μg/mL (F_0 and F represent the fluorescence intensity of the solution as a whole before and after the addition of trypsin.)

CNPs shorten the distance allowing the transfer of fluorescent energy from FAM to CNPs [40,41]. FAM was excited as a fluorophore and became an energy donor, and the fluorescence was quenched by almost 100% after adding CNPs, which indicated that the energy difference between the vibrational levels of the donor FAM's ground state and the first excited state and the vibrational levels of the acceptor CNPs had a high degree of overlap [42,43].

The corresponding Stern-Volmer curve is presented in Fig. 2D, where F_0 and F represent the fluorescence intensity at 520 nm before and after adding the quenching CNPs, respectively [44]. The slope K_{SV} value was 0.4255 (μg/mL), and it was concluded that the concentration of the quencher was 2.35 μg/mL when the fluorescence intensity of $1/K_{SV}$ was quenched to 50%. In addition, the Stern-Volmer diagram exhibited an upward curving trend, indicating that the FAM fluorophore undergoes dynamic quenching and static quenching.

3.2. Response of CNPs-peptide fluorescence sensor to trypsin

We studied reaction kinetics involving trypsin. Fig. 3A shows plots of fluorescence intensity at 520 nm versus the reaction time for the ensemble of CNPs and Arg_6-FAM in the presence of different concentrations of trypsin. Before addition of trypsin, the fluorescence intensity remained essentially unchanged. In the presence of trypsin, the overall fluorescence intensity of the solution increased, and the reaction reached equilibrium in approximately 30 min [45]. In addition, the fluorescence intensity of the solution increased with elevating trypsin concentration.

Next, experiments were conducted to investigate whether the CNPs/Arg_6-FAM complex can be used to establish a method for detecting trypsin content. The fluorescence of the CNPs/Arg_6-FAM complex was very weak, as described above. However, arginine can be hydrolyzed by the specific catalytic action of trypsin, which caused the cleavage of CNPs and Arg_6-FAM, disrupted FRET, whereas the FAM emission peak recovered, leading to a gradual increase in fluorescence intensity of the solution [46,47]. The initial PBS containing Arg_6-FAM (0.1 nM) and CNPs (20 μg/mL) exhibited very weak fluorescence, as depicted in Fig. 3B. The fluorescence intensity of the whole solution gradually recovered with increasing trypsin concentration. As shown in the inset of Fig. 3B, this fluorescence recovery change can be recognized by the naked eye. A photograph of the overall solution (under UV light irradiation) in both the absence and presence of trypsin is also illustrated. These results clearly manifested that a continuous fluorescence turn-on assay for trypsin can be established with the ensemble of CNPs and Arg_6-FAM described here.

Fig. 3C presents the fluorescence responses of CNPs/Arg_6-FAM complexes to trypsin in PBS (pH = 8.0) at different concentrations. Trypsin is also a highly efficient biocatalyst that can hydrolyze > 10^5 peptide substrate molecules very rapidly [48]. Therefore, compared with conventional fluorescent immunoassay methods, the sensitivity of enzyme-linked amplification fluorescence immunoassays can generally be superior by two orders of magnitude [49]. It can be seen from Fig. 3C that the higher the concentration of trypsin in the solution, the greater the fluorescence intensity recovery of the reaction system. The fluorescence intensity was directly proportional to trypsin concentrations over the range 2–20 μg/mL, with a linear equation of $(F-F_0)/F_0 = 0.0325$ [trypsin]+4.135 ($R^2 = 0.998$). The detection limit (3σ/S, in which σ is the standard deviation of blank measurements, $n = 7$, and S is the slope of the linear equation) was 0.7 μg/mL. Poon et al. [50] used graphene quantum dot materials to

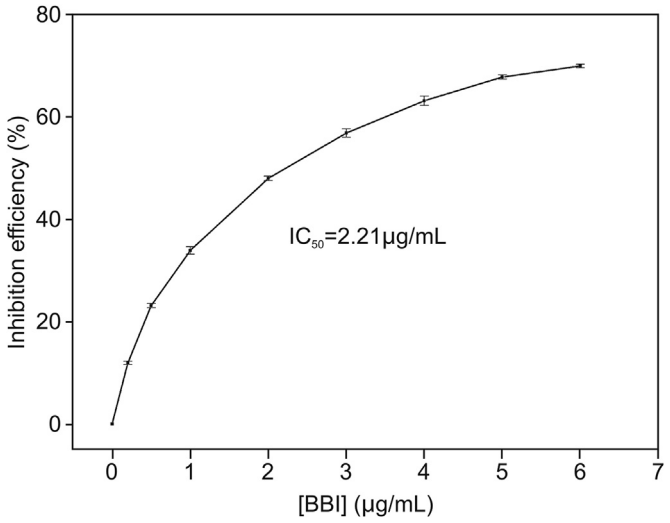

Fig. 4. Plot of the inhibition efficiency of BBI toward trypsin versus the concentration of BBI. Measurements were performed with Arg_6-FAM (0.1 nM), CNPs (20 μg/mL), trypsin (10 μg/mL), and different concentrations of BBI (0, 0.2, 0.5, 1, 2, 3, 4, 5, and 6 μg/mL) in PBS (2.0 mM, pH = 8.0, $[Ca^{2+}]$ = 10 μM).

obtain a linear range of 0–6 μg/mL, also employing the FRET principle. In contrast, we have demonstrated a wider linear range by using CNPs.

3.3. Detection of trypsin inhibitor

The pancreatic-catalyzed hydrolysis of Arg_6-FAM might be delayed after adding the corresponding trypsin inhibitor. It could be anticipated that after the addition of the trypsin inhibitor, the degree of fluorescence enhancement of the trypsin-containing CNPs/Arg_6-FAM complex might decrease. BBI from soybean was selected as an example of an inhibitor to demonstrate that CNPs/Arg_6-FAM as a whole can also be used for screening for trypsin inhibitors [51]. Fig. 4 illustrates the inhibition efficiency after adding different amounts of BBI [$(1\text{-}F/F_0) \times 100$, where F_0 and F represent the fluorescence intensities at 520 nm before and after addition of the BBI, respectively] at 520 nm of a mixed solution of Arg_6-FAM (0.1 nM), CNPs (20 μg/mL), and trypsin (10 μg/mL) [52]. The corresponding IC_{50} value (inhibitor concentration resulting in reduction of 50% enzymic activity) was estimated to be 2.21 μg/mL. This result demonstrated that the CNPs/Arg_6-FAM complex approach was equally applicable to high throughput screening of trypsin inhibitors.

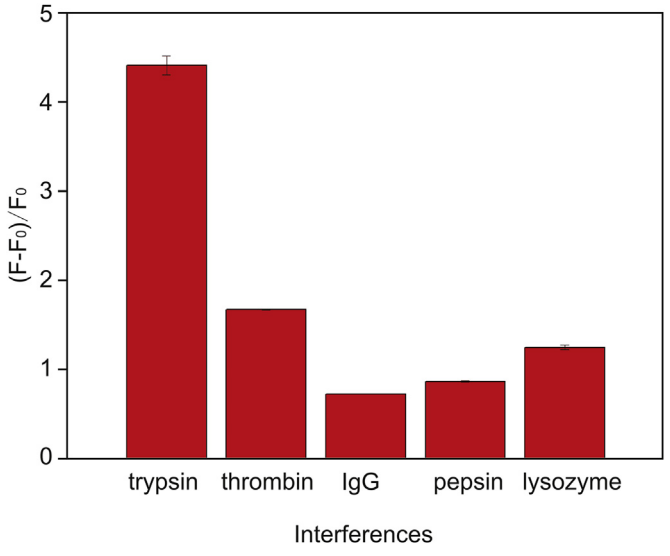

Fig. 5. Recovery efficiency of the CNPs/Arg_6-FAM system in the presence of trypsin, thrombin, IgG, pepsin, and lysozyme. The concentration of each protein was 10 μg/mL.

Table 1
Measurements of trypsin in human urine samples.

Sample	Added (μg/mL)	Found (μg/mL)	Recovery (%)	RSD (%, n = 3)
1	0	-	-	-
	5	5.02	100	1.41
	10	10.1	101	2.36
	15	15.45	103	3.05
2	0	-	-	-
	5	4.89	97.7	1.90
	10	10.2	102	1.41
	15	15.15	101	3.89
3	0	-	-	-
	5	5.01	100	2.10
	10	10.3	103	3.58
	15	15.6	104	4.28

Note: "-" stands for "not detected".

3.4. Selectivity study

We explored the selectivity of our sensor by screening the spectral responses of certain molecular species coexisting with trypsin in biological systems, including lysozyme, thrombin, pepsin, and IgG under the same conditions [53]. The biosensor exhibited selective fluorescence recovery for trypsin (10 μg/mL) compared to other interferents (10 μg/mL), as can be seen in Fig. 5. In order to avoid interference from thrombin responses to the CNPs/Arg_6-FAM fluorescent aptamer system, a thrombin-specific inhibitor peptide P13 could be added [54].

3.5. Detection of trypsin in human urine samples

To evaluate the accuracy and selectivity of this biosensor, we measured different concentrations of trypsin in urine samples, and the obtained data are listed in Table 1. According to the standard curve and the regression equation, the trypsin content in the urine samples was derived [55], and the RSD was obtained from a series of three samples. The average recovery rate test was carried out using the standard addition method [56], and the recovery rate was between 97.7% and 104%. In addition, the above results demonstrated the potential applicability of the CNPs/Arg_6-FAM system in detecting trypsin activity in human urine samples.

4. Conclusion

In summary, a convenient and sensitive fluorometric sensor assembled FAM-labelled peptide with CNPs for detecting trypsin in urine has been successfully demonstrated here. In comparison with previously reported trypsin detection strategies, our method was highly selective due to the fluorescence response, which was only initiated by specific cleavage of the synthetic trypsin substrate peptide. It should be noted that this proposed method detected trypsin without complicated procedures and exhibited a wide linear range encompassing 2–20 μg/mL. Furthermore, the detection limit was 0.7 μg/mL, which is 0.8% of the average trypsin level in the urine of patients with acute pancreatitis. As far as we know, this is the first example of a pancreatic enzyme biosensing method based on CNPs, which may provide a useful strategy for pancreatic disease screening. In addition, the current sensor demonstrates a significant potential for developing new methods to detect other

important proteases.

Declaration of competing interest

The authors declare that there are no conflicts of interest.

References

[1] Y.B. Liu, F.M. Zhang, X. He, et al., A novel and simple fluorescent sensor based on AgInZnS QDs for the detection of protamine and trypsin and imaging of cells, Sensor. Actuator. B Chem. 294 (2019) 263–269.
[2] W.X. Xue, G.X. Zhang, D.Q. Zhang, A sensitive colorimetric label-free assay for trypsin and inhibitor screening with gold nanoparticles, Analyst 136 (2011), 3136–3134.
[3] W.X. Xue, G.X. Zhang, D.Q. Zhang, et al., A new label-free continuous fluorometric assay for trypsin and inhibitor screening with tetraphenylethene compounds, Org. Lett. 12 (2010) 2274–2277.
[4] X. Liu, Y. Li, L. Jia, et al., Ultrasensitive fluorescent detection of trypsin on the basis of surfactant–protamine assembly with tunable emission wavelength, RSC Adv. 6 (2016) 93551–93557.
[5] W. Liu, H.H. Li, et al., A label-free phosphorescence sensing platform for trypsin based on Mn-ZnS QDs, RSC Adv. 7 (2016) 26930–26934.
[6] M.A. Seia, P.W. Stege, S.V. Pereira, et al., Silica nanoparticle-based microfluidic immunosensor with laser-induced fluorescence detection for the quantification of immunoreactive trypsin, Anal. Biochem. 463 (2014) 31–37.
[7] X.D. Lou, L.Y. Zhang, J.G. Qin, et al., Colorimetric sensing of α-amino acids and its application for the "label-free" detection of protease, Langmuir 26 (2010) 1566–1569.
[8] M.M. Dong, H.L. Qi, S.G. Ding, et al., Electrochemical determination of trypsin using a heptapeptide substrate self-assembled on a gold electrode, Microchim. Acta. 182 (2014) 43–49.
[9] F.P. Shi, L. Wang, Y. Li, et al., A simple "turn-on" detection platform for trypsin activity and inhibitor screening based on N -acetyl- l -cysteine capped CdTe Quantum Dots, Sensor. Actuator. B Chem. 255 (2018) 2733–2741.
[10] B.Y. Tang, Y. Yang, G.F. Wang, et al., A simple fluorescent probe based on a pyrene derivative for rapid detection of protamine and monitoring of trypsin activity, Org. Biomol. Chem. 13 (2015) 8708–8712.
[11] J. Wen, Y.Q. Xu, H.J. Li, et al., Recent applications of carbon nanomaterials in fluorescence biosensing and bioimaging, Chem. Commun. 51 (2015) 11346–11358.
[12] L.H. Ding, Z.Y. Zhao, D.J. Li, et al., An "off-on" fluorescent sensor for copper ion using graphene quantum dots based on oxidation of l-cysteine, Spectrochim. Acta A. 214 (2019) 320–325.
[13] H.P. Liu, T. Ye, C.D. Mao, Fluorescent carbon nanoparticles derived from candle soot, Angew. Chem. Int. Ed. Engl. 46 (2007) 6473–6475.
[14] M. Kakunuri, C.S. Sharma, Candle soot derived fractal-like carbon nanoparticles network as high-rate lithium ion battery anode material, electrochim, Acta 180 (2015) 353–359.
[15] H.L. Li, Y.W. Zhang, L. Wang, et al., Nucleic acid detection using carbon nanoparticles as a fluorescent sensing platform, Chem. Commun. 47 (2011) 961–963.
[16] S.L. Hu, Y.G. Dong, J.L. Yang, et al., Simultaneous synthesis of luminescent carbon nanoparticles and carbon nanocages by laser ablation of carbon black suspension and their optical limiting properties, J. Mater. Chem. 22 (2012) 1957–1961.
[17] W. Zhang, G.F. Wang, N. Zhang, et al., Preparation of carbon nanoparticles from candle soot, Chem. Lett. 38 (2009) 28–29.
[18] H.L. Li, J.F. Zhai, X.P. Sun, Sensitive and selective detection of silver(I) ion in aqueous solution using carbon nanoparticles as a cheap, effective fluorescent sensing platform, Langmuir 27 (2011) 4305–4308.
[19] Y.X. Hou, Q.J. Lu, J.H. Deng, et al., One-pot electrochemical synthesis of functionalized fluorescent carbon dots and their selective sensing for mercury ion, Anal. Chim. Acta 866 (2015) 69–74.
[20] D. Geißler, S. Linden, K. Liermann, et al., Lanthanides and quantum dots as förster resonance energy transfer agents for diagnostics and cellular imaging, Inorg. Chem. 53 (2013) 1824–1838.
[21] S. Singh, D. Singh, S.P. Singh, et al., Candle soot derived carbon nanoparticles: assessment of physico-chemical properties, cytotoxicity and genotoxicity, Chemosphere 214 (2019) 130–135.
[22] X. Gao, G.C. Tang, Y. Li, et al., A novel optical nanoprobe for trypsin detection and inhibitor screening based on Mn-doped ZnSe quantum dots, Anal. Chim. Acta 743 (2012) 131–136.
[23] I.M. Khan, S. Zhao, S. Niazi, et al., Silver nanoclusters based FRET aptasensor for sensitive and selective fluorescent detection of T-2 toxin, Sensor. Actuator. B Chem. 277 (2018) 328–335.
[24] S. Srinivasan, V. Ranganathan, M.C. DeRosa, et al., Label-free aptasensors based on fluorescent screening assays for the detection of Salmonella typhimurium, Anal. Biochem. 559 (2018) 17–23.
[25] L.F. Zhang, H.Y. Qin, W.W. Cui, et al., Label–free, turn–on fluorescent sensor for trypsin activity assay and inhibitor screening, Talanta 161 (2016) 535–540.
[26] M. Li, X.J. Zhou, S.W. Guo, et al., Detection of lead (II) with a "turn-on" fluorescent biosensor based on energy transfer from CdSe/ZnS quantum dots to graphene oxide, Biosens. Bioelectron. 43 (2013) 69–74.
[27] L.Z. Hu, S. Han, S. Parveen, et al., Highly sensitive fluorescent detection of trypsin based on BSA-stabilized gold nanoclusters, Biosens. Bioelectron. 32 (2012) 297–299.
[28] Y. Song, X.W. Kang, N.B. Zuckerman, et al., Ferrocene-functionalized carbon nanoparticles, Nanoscale 3 (2011) 1984–1989.
[29] W. Zhang, G.F. Wang, N. Zhang, et al., Preparation of carbon nanoparticles from candle soot, Chem. Lett. 38 (2009) 28–29.
[30] S.C. Ray, A. Saha, N.R. Jana, et al., Fluorescent carbon nanoparticles: synthesis, characterization, and bioimaging application, J. Phys. Chem. C 113 (2009) 18546–18551.
[31] R.P. Singh, G. Sharma, Sonali, et al., Chitosan-folate decorated carbon nanotubes for site specific lung cancer delivery, Mater. Sci. Eng. C 77 (2017) 446–458.
[32] D.G. Deryabin, L.V. Efremova, A.S. Vasilchenko, et al., A zeta potential value determines the aggregate's size of penta-substituted [60] fullerene derivatives in aqueous suspension whereas positive charge is required for toxicity against bacterial cells, J. Nanobiotechnol. 13 (2015) 1–13.
[33] S. Singh, P.K. Bairagi, N. Verma, Candle soot-derived carbon nanoparticles: An inexpensive and efficient electrode for microbial fuel cells, Electrochim. Acta 264 (2018) 119–127.
[34] M.R. Mulay, A. Chauhan, S. Patel, et al., Candle soot: journey from a pollutant to a functional material, Carbon 144 (2019) 684–712.
[35] X.G. Gu, G. Yang, G.X. Zhang, et al., A new fluorescence turn-on assay for trypsin and inhibitor screening based on graphene oxide, ACS Appl. Mater. Interfaces 3 (2011) 1175–1179.
[36] M.K. Wang, D.D. Su, G.N. Wang, et al., A fluorometric sensing method for sensitive detection of trypsin and its inhibitor based on gold nanoclusters and gold nanoparticles, Anal. Bioanal. Chem. 410 (2018) 6891–6900.
[37] T.T. Feng, D. Feng, W. Shi, et al., A graphene oxide-peptide fluorescence sensor for proteolytically active prostate-specific antigen, Mol. Biosyst. 8 (2012) 1441–1445.
[38] A.S.-Y. Law, M.C.-L. Yeung, V.W.-W. Yam, Arginine-rich peptide-induced supramolecular self-assembly of water-soluble anionic alkynylplatinum(II) complexes: A continuous and label-free luminescence assay for trypsin and inhibitor screening, ACS Appl. Mater. Interfaces 9 (2017) 41143–41150.
[39] Y.H. Wang, L. Bao, Z.H. Liu, et al., Aptamer biosensor based on fluorescence resonance energy transfer from upconverting phosphors to carbon nanoparticles for thrombin detection in human plasma, Anal. Chem. 83 (2011) 8130–8137.
[40] H. Yang, W.Y. Zhao, S. Deng, et al., Intrinsic conformation-induced fluorescence resonance energy transfer aptasensor, ACS Appl. Bio Mater. 5 (2020) 2552–2559.
[41] K.Q. Yang, J.J. Zhao, L.L. Zhang, In situ ratiometric fluorescence imaging for tracking targeted delivery and release of anticancer drug in living tumor cells, ACS Appl. Bio Mater. 2 (2019) 4687–4692.
[42] G. Musile, E.F.D. Palo, S.A. Savchuk, et al., A novel low-cost approach for the semi-quantitative analysis of carbohydrate-deficient transferrin (CDT) based on fluorescence resonance energy transfer (FRET), Clin. Chim. Acta 495 (2019) 556–561.
[43] M. Wang, K. Su, J. Cao, et al., "Off-On" non-enzymatic sensor for malathion detection based on fluorescence resonance energy transfer between β-cyclodextrin@Ag and fluorescent probe, Talanta 192 (2019) 295–300.
[44] S. Gogoi, R. Khan, Fluorescence immunosensor for cardiac troponin T based on Förster resonance energy transfer (FRET) between carbon dot and MoS2 nanocouple, Phys. Chem. Chem. Phys. 20 (2018) 16501–16509.
[45] T. Zauner, R. Berger-Hoffmann, K. Müller, et al., Highly adaptable and sensitive protease assay based on fluorescence resonance energy transfer, Anal. Chem. 83 (2011) 7356–7363.
[46] H.Y. Chen, A.J. Fang, Y.Y. Zhang, et al., Silver triangular nanoplates as an high efficiently FRET donor-acceptor of upconversion nanoparticles for ultrasensitive "Turn on-off" protamine and trypsin sensor, Talanta 174 (2017) 148–155.
[47] T.T. Feng, H.M. Ma, Fluorescence sensing of adenosine deaminase based on adenosine induced self-assembly of aptamer structures, Analyst 138 (2013) 2438–2442.
[48] X.Y. Lin, L. Cui, Y.S. Huang, et al., Carbon nanoparticle-protected aptamers for highly sensitive and selective detection of biomolecules based on nuclease-assisted target recycling signal amplification, Chem. Commun. 50 (2014) 7646–7648.
[49] J.-G. You, W.-L. Tseng, Peptide-Induced aggregation of glutathione-capped gold nanoclusters: A new strategy for designing aggregation-induced enhanced emission probes, Anal. Chim. Acta 1078 (2019) 101–111.
[50] C.-Y. Poon, Q.H. Li, J. L Zhang, et al., FRET-based modified graphene quantum dots for direct trypsin quantification in urine, Anal. Chim. Acta 917 (2016) 64–70.
[51] X.T. Hu, J.Y. Shi, Y.Q. Shi, et al., A ratiometric fluorescence sensor for ultra-

sensitive detection of trypsin inhibitor in soybean flour using gold nanocluster@carbon nitride quantum dots, Anal. Bioanal. Chem. 411 (2019) 3341–3351.
[52] D. Sato, T. Kato, Novel fluorescent substrates for detection of trypsin activity and inhibitor screening by self-quenching, Bioorg. Med. Chem. Lett 26 (2016) 5736–5740.
[53] M.M. Wu, X.Y. Wang, K. Wang, et al., An ultrasensitive fluorescent nanosensor for trypsin based on upconversion nanoparticles, Talanta 174 (2017) 797–802.
[54] F.Y. Chen, G.R. Huang, Mechanism and inhibition kinetics of peptide P13 as thrombin inhibitor, Int. J. Biol. Macromol. 150 (2020) 1046–1052.
[55] S.Y. Zhang, C. Chen, X.F. Qin, et al., Ultrasensitive detection of trypsin activity and inhibitor screening based on the electron transfer between phosphorescence copper nanocluster and cytochrome c, Talanta 189 (2018) 92–99.
[56] X.Y. You, Y.H. Li, B.P. Li, et al., Gold nanoclusters-based chemiluminescence resonance energy transfer method for sensitive and label-free detection of trypsin, Talanta 147 (2016) 63–68.